Numerical Study on Dynamic Loading Response of Mid- and High-Strength Aluminum-CFRP Hybrid Rails

Zohreh Asaee*, John Montesano, and Michael Worswick
Department of Mechatronics and Mechanical Engineering, University of Waterloo, Canada
* Corresponding author (zohreh.asaee@uwaterloo.ca)

ABSTRACT

The performance of hybrid hat-section rails comprising aluminum alloy and unidirectional carbon fiber reinforced plastic (CFRP) patches was examined using numerical simulations of dynamic three-point bend loading. Two grades of aluminum, mid-strength 5000-series and high-strength 7000-series, were considered to investigate the effect of hybridization of different strength ranges of these alloys. The results were compared against those of the reference aluminum-only rail with similar weight. The models predict that the hybridization of mid-strength aluminum considerably increases the first peak load and absorbed energy under three-point bend dynamic loading conditions. In the case of high-strength aluminum, it was shown that the hybrid rail attains a higher peak load in comparison to the metal-only rail; however, the metal rail (with similar weight to the hybrid) has a higher energy absorption capacity than the hybrid rail. Several layup configurations of the composite reinforcement were considered to investigate their effect on the performance of the hybrid beams. It was shown that the $[\pm 45]_s$ layup configuration had the best performance amongst the considered configurations.

KEYWORDS: *Metal-composite hybrid structure, Dynamic loading, Numerical simulation, Carbon fiber reinforced composite.*

1 INTRODUCTION

During the last decade, there has been considerable effort to increase the efficiency of vehicles to meet legislated fuel economy standards and emission reduction targets. One of the key solutions to improve automotive efficiency is to decrease vehicle weight ((German and Lutsey, 2012)).

In terms of light weighting, there is a fierce competition underway between composite and metal suppliers within the automotive industry ((Marsh, 2014)). Considerable numbers of vehicle structures are designed based on steel and aluminum materials ((Lindberg, 2016)), while more recently others have focused on both metallic and composite materials (Boeriu, 2015). The concept of multi-material structures for vehicle light weighting is to use the lightest material with optimal performance in each location within the automotive body structure (Marsh, 2014). Hybrid multi-material metal/composite structures represent one type of solution that has been evaluated extensively in the aerospace ((Dutton *et al.*, 2004)) and racing sectors (Savage, 2010), but has received less attention in the automotive sector to-date.

Several studies have been conducted on the mechanical performance of hybrid systems under various loading conditions (Abu Talib *et al.*, 2010; Cao *et al.*, 2009; Hong *et al.*, 2010; Lee *et al.*, 2004; Sun *et al.*, 2018; Zhu *et al.*, 2018). In most of these studies, the mechanical behavior of the metal/composite hybrid materials was investigated under quasi-static loading. Zhu *et al.* (2018) conducted research on the energy absorption capacity of metal, composite and metal/composite hybrid structures. Aluminum tubes were reinforced by carbon fiber reinforced plastic (CFRP) and tested under oblique quasi-static axial loading. It was observed that hybrid configurations offered higher energy absorption capacity to meet crashworthiness requirements among all configurations.

The aim of the current study is to investigate the effects of hybridization on the performance of mid-strength and high-strength aluminum alloys under dynamic crush loading. Two grades of aluminum AA5182-O (mid-strength) and AA7075-T6 (high-strength) were considered and were reinforced using HexPly 8552 high strength unidirectional carbon fiber/epoxy laminates in hat-shaped cross-section rails. Using commercial software, a finite element (FE) model was developed to numerically simulate the behavior of the rails under dynamic three-point bend loading. Force and absorbed energy *versus* displacement were compared for several groups of aluminum-only and hybrid configurations. In order to perform an unbiased comparison, aluminum-only rails with similar mass to the hybrid configurations were simulated and their relative performance was compared. Moreover, the effects of the composite layup configuration were studied by considering three different layup configurations of the CFRP reinforcements.

2 NUMERICAL MODELLING

Three-point bending simulation of the hybrid rails was performed using the commercial finite element software *LS-DYNA R.9.0.1*. A perspective view of the FE model and the cross-section of the hybrid channel are presented in Figure 1. All of the components considered in the FE model are labeled in the perspective view. The hybrid channel consists of a metal hat section reinforced with a composite patch bonded to the inside of the hat section. In order to provide a closed section with more structural stability, a metal backing plate was attached to the hat channel beam using rivet constraint available in *LS-DYNA*. The material of the backing plate was the same alloy as used in the hat channel. The channel length and support span were 600 mm and 365 mm, respectively. The diameter of impactor and supports were 100 mm and 50 mm, respectively.

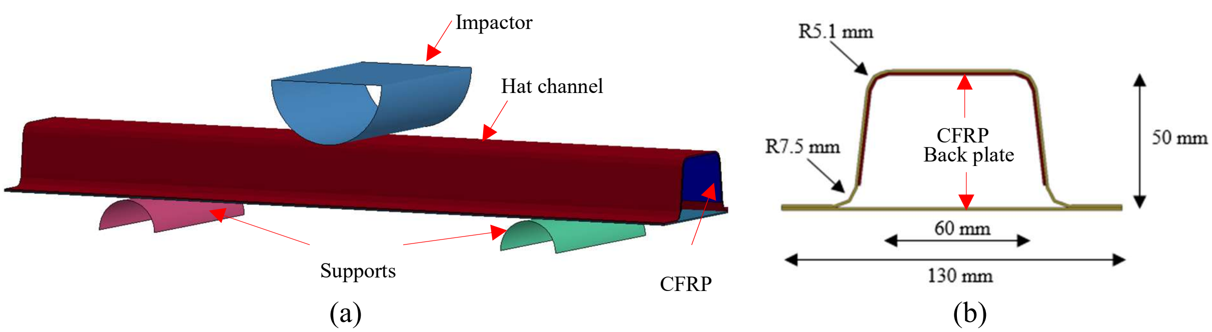

Figure 1: (a) Perspective view and (b) cross-section of hybrid configuration in the simulated FE model

As explained earlier, two grades of aluminum were considered for the metal section, AA5182-O (medium strength) and AA7075-T6 (high strength). The thickness of the metal and hybrid beams is 1 mm and 2 mm, respectively. The aluminum material was simulated using the Barlat YLD-2000 (Barlat *et al.*, 2003) non–quadratic yield function. Both grades of aluminum were simulated using rate-dependent behavior. The flow stress curves of two grades of aluminum are presented in Figure 2. The failure and extent of damage in the aluminum materials were simulated using the generalized incremental stress-state dependent damage model (GISSMO) (Neukamm *et al.*, 2009). The GISSMO model predicts failure based on an incremental damage accumulation according to the following formula:

$$\Delta D = \frac{n \times D^{\left(1-\frac{1}{n}\right)}}{\varepsilon_f} \Delta\varepsilon_p \tag{1}$$

where D is a damage index, n is an exponent for nonlinear damage accumulation, ε_f and $\Delta\varepsilon_p$ are the effective plastic strain at failure, expressed as a function of stress triaxiality, and the incremental effective plastic strain, respectively. When D reaches the value of unity, the respective element fails and is subsequently deleted.

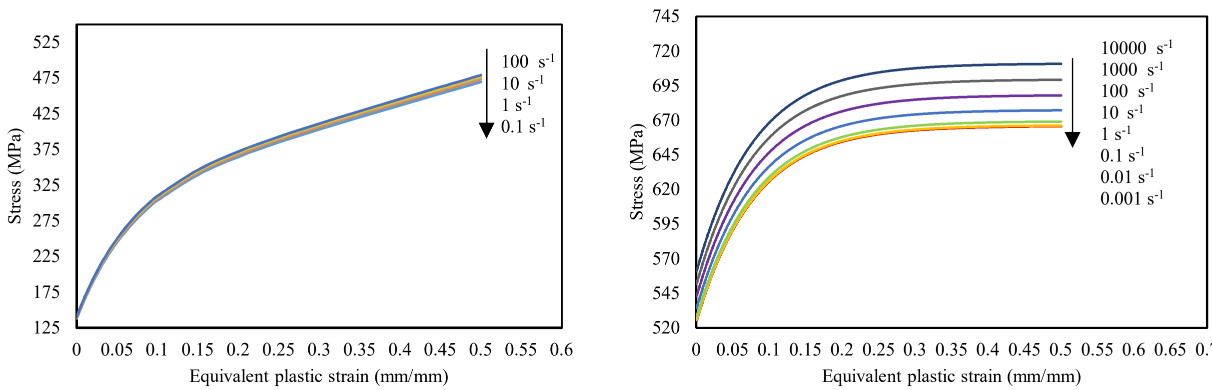

(a) (b)

Figure 2: Flow stress curves corresponding to (a) AA5182-O (Rahmaan *et al.*, 2016) and (b) AA7075-T6 (Rahmaan *et al.*, 2017)

The laminated composite patch simulated in this study was comprised of HexPly 8552 high strength unidirectional carbon fiber/epoxy plies (HEXCEL, 2016). The CFRP patch was simulated using layered shell elements with defined linear elastic orthotropic plies and MAT54/55 (Hallquist, 2013). Material integration points were defined through the shell thickness. MAT54/55 offers two types of failure criteria including Chang-Chang (1987) and Tsai-Wu (1971). The failure criteria implemented in this study for both fiber and matrix failure modes, in tension and compression, is summarized as follows:

$$e_{fT}^2 = \left(\frac{\sigma_{11}}{X_T}\right)^2 + \beta\left(\frac{\tau_{12}}{S_c}\right)^2 - 1, \tag{2}$$

$$e_{fC}^2 = \left(\frac{\sigma_{11}}{X_C}\right)^2 - 1, \tag{3}$$

$$e_{mC,mT}^2 = \frac{\sigma_{22}^2}{Y_C Y_T} + \left(\frac{\tau_{12}}{S_C}\right)^2 + \frac{(Y_C - Y_T)\sigma_{22}}{Y_C Y_T} - 1 \tag{4}$$

where σ_{ij}*'s* and τ_{12} are the in-plane stresses and shear stress in the ply, and β, taken as zero in this study, is the contribution factor for the shear term in the tensile fiber mode. e_{fT}, e_{fC}, e_{mT} and e_{mC} are the damage indices for the longitudinal tensile, longitudinal compression, transverse tensile and compression modes, respectively. X_T, X_C, Y_T, Y_C, and S_C are the longitudinal tensile, longitudinal compression, transverse tensile, transverse compression, and shear strength, respectively. The elements were deleted when a failure criterion was met at all integration points in the element. The material properties of the CFRP are presented in Table 1.

For the hybrid configurations, three different layup sequences of CFRP were considered to examine the effects of layup orientation on the dynamic response of the hybrid beams, specifically $[0/90]_s$, $[0/45]_s$, and $[\pm 45]_s$. In order to compare the hybrid structure to a metal-only structure of equal mass, simulations were also performed considering aluminum rails of 1.2 mm thickness that matches the mass of the hybrid configurations.

Table 1 Mechanical properties of HexPly 8552 composite (Cherniaev *et al.,* 2018)

Density (kg/mm^3)	**Longitudinal Young's modulus (MPa)**	**Transverse Young's modulus (MPa)**	**Poison's ratio**	**Shear modulus (MPa)**
1.58×10^{-6}	165000	9000	0.0185	5600
Longitudinal compressive strength, X_C (MPa)	**Longitudinal tensile strength, X_T (MPa)**	**Transverse compressive strength, Y_C (MPa)**	**Transverse tensile strength, Y_T (MPa)**	**Shear strength (MPa), S_C**
1590	2560	185	73	90

The impactor and two supports were simulated as rigid bodies. The mass of the impactor and crush speed were assigned as 855 kg and 7.0 m/s, respectively, to simulate the crush tests performed by the impact sled at the University of Waterloo (Omer *et al.*, 2017). Penalty function-based contacts were defined between the impactor, the two supports, and the specimen. In addition, a tied contact constraint was defined between the metal hat beam and the composite counterparts to model the interfacial bond. The tied contact was simulated using a tie-break contact available in *LS-DYNA.* This penalty-based contact condition allows for the separation of the two parts. It should be noted that the delamination is not tracked for post processing purposes using the tied-break contact type and future efforts will consider cohesive zone approaches.

3 RESULTS AND DISCUSSION

The metal and hybrid beams using the AA5182-O and AA7075-T6 alloys underwent dynamic three-point bend loading. The general deformed shape is shown in Figure 3. The beams in both cases, *i.e.* metal-only and hybrid, folded at the center of the beam without wrapping around the impactor. The deformed shape of the medium strength AA-5182-O was similar to that of the AA7075-T6 beams. However, greater extent of fracture was observed for the AA7075-T6 rails under the simulated loading condition. The beams folded directly under the impactor.

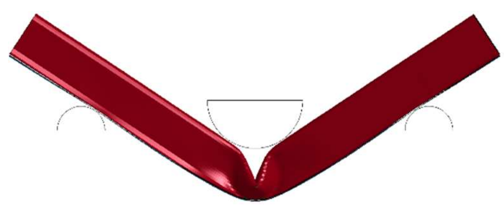

Figure 3: The deformed shape of hybrid beams made of AA7075-T6 and $[\pm45]_s$ CFRP laminate at the displacement of 135 mm

Figure 4 shows the predicted force-displacement and absorbed energy-displacement curves of the simulations performed with the AA5182-O alloy. Examination of Figure 4 showed that the metal-only beams (1 mm thickness) exhibited a peak load of 3581 N at an impactor displacement of 10.7 mm, whereas the hybrid beams displayed a peak load of 7543 N at an impactor displacement of 17.7 mm. (Note that comparison with the 1.2 mm metal-only rail of similar weight is presented below.) Total energy absorbed for metal and hybrid channels were 218 J and 387 J, respectively. The results show that for AA5182-O, the higher strength composite greatly increases peak load and energy absorption by 108% and 77%. Moreover, the predictions indicate that the hybrid beam with $[\pm45]_S$ layup configuration showed the highest energy absorption capacity amongst all investigated layup configurations.

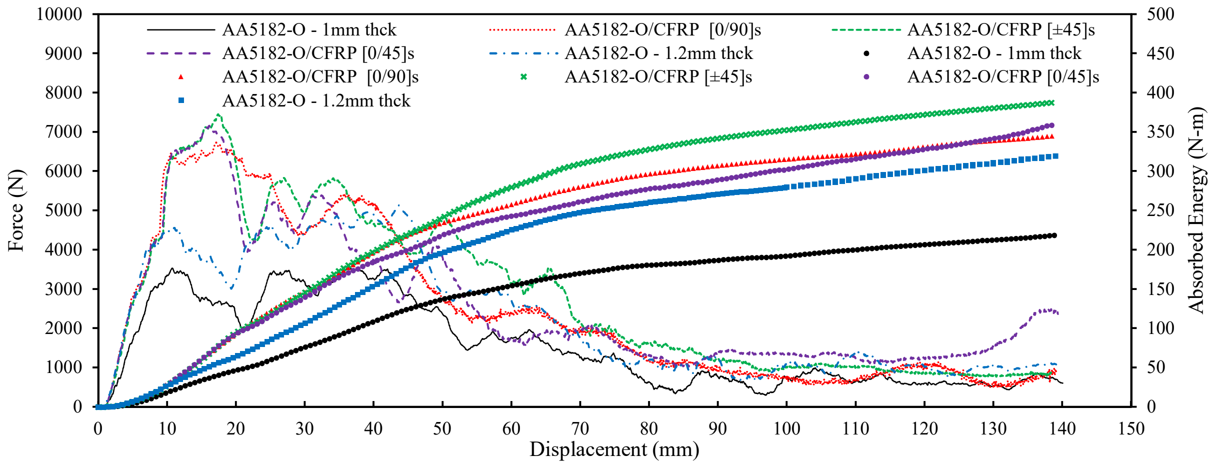

Figure 4: Force and absorbed energy against displacement of the AA5182-O aluminum (1mm and 1.2mm thicknesses) and three AA5182-O/CFRP hybrid configurations

Figure 5 represents the force-displacement and absorbed energy-displacement curves for the AA7075-T6 cases under dynamic three-point bend loading. The 1 mm AA7075-T6 configuration displayed a peak load of 8370 N at a punch displacement of 7.7 mm, while the peak load of 13372 N for the AA7075/CFRP [±45]$_S$ case occurred at a displacement of 10.7 mm. Similar to the results of the AA5182-O groups, the layup configuration of [±45]$_S$ occured the best performance among the investigated configurations. Due to the reinforcement effect, the peak load and energy absorption of the hybrid in comparison to 1 mm metal-only rail increased by 63% and 40%, respectively.

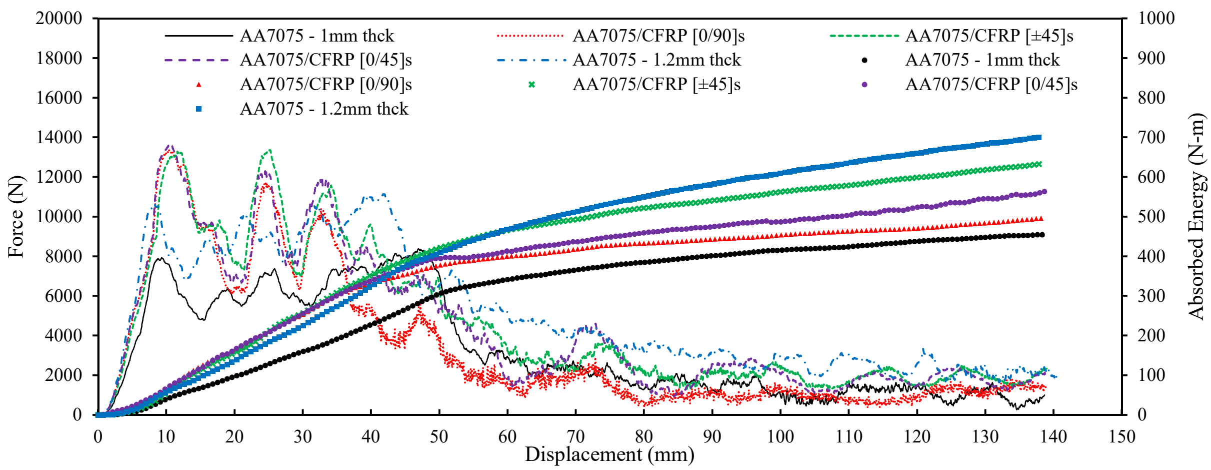

Figure 5: Force and absorbed energy against displacement of the AA7075-T6 aluminum (1mm and 1.2mm thicknesses) and three AA7075/CFRP hybrid configurations

The extent of crack and damage progression of metal-only and hybrid beams from the AA7075-T6 group are presented in Figure 6. In the metal-only beam, fracture occurred mainly in the top of the section near the impactor and on the edges. In the hybrid configuration, the contribution of the composite patch to the load carrying capacity prevented crack formation in the metal section. Whereas in the composite part, the crack was mainly observed on the edges and the wall. It can be concluded that the composite patch contributed to higher energy absorption in the wall and on the edge of hat-section beam.

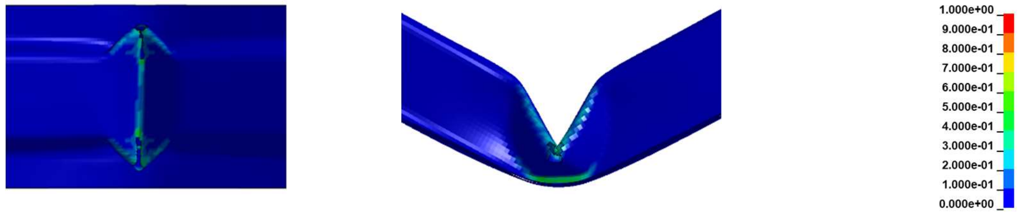

(a) Plan view (b) Side view

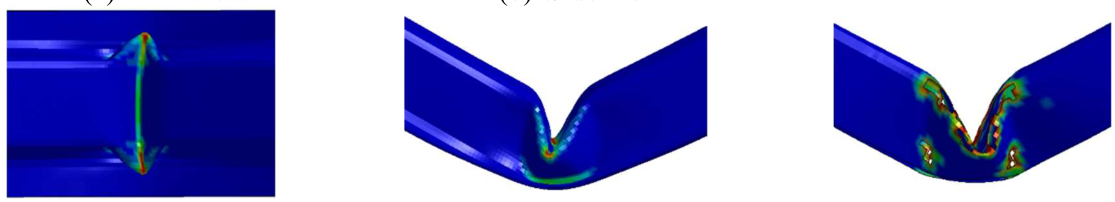

(c) Plan View (d) Side view (e) Side view

Figure 6: Predicted damage index and crack extension in: (a,b) the AA7075-T6 aluminum-only rail; (c,d) the metal constituent and, (e) composite patch of the AA7075-T6 hybrid rail

A comparison of the performance of the mid-strength and high-strength metal-only and hybrid beams is depicted in Figure 7. The results for the hybrid rails were compared to those of the aluminum-only rails with equal weight. For the mid-strength (AA5182-O) aluminum, the hybrid configuration showed an increase in both peak load and energy absorption capacity in comparison to the corresponding metal-only case with similar mass. For AA7075-T6, the hybrid patch increased peak load due to the reinforcement effect, but the energy absorption was higher for corresponding 1.2 mm metal-only rail.

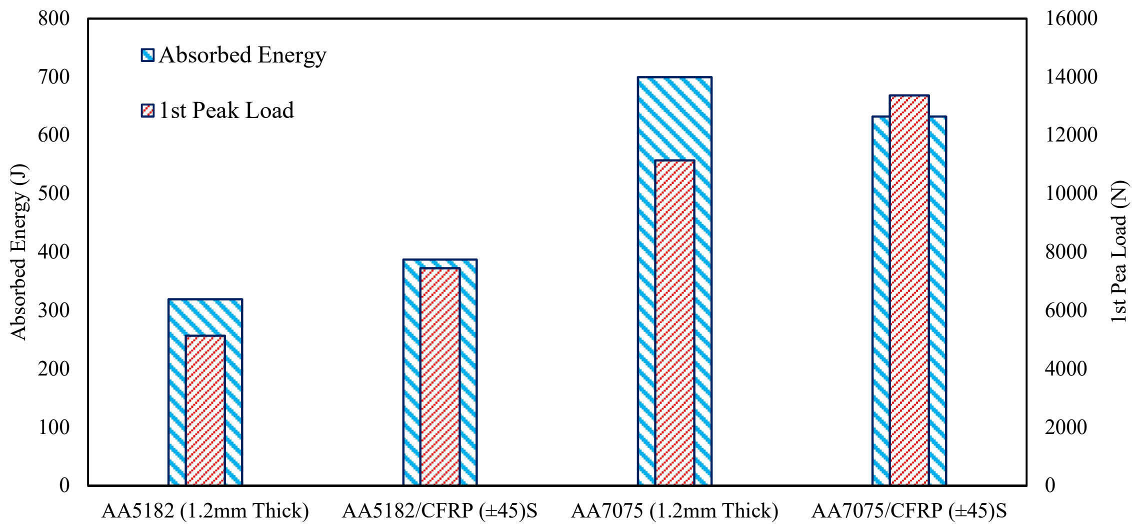

Figure 7: Peak load and absorbed energy of the metal-only and hybrid rails made of AA5182-O and AA7075-T6

4 CONCLUSION

The results outlined in this work present the effects of hybridization on the performance of the mid-strength and high-strength aluminum alloys. In the case of mid-strength alloy, the composite patch increased the peak load and absorbed energy by 108% and 77%. The hybridization of the mid-strength aluminum alloy was more effective than the hybridization of the high-strength aluminum alloy. For the

AA7075-T6 group, the composite patch increased the peak load, however, the absorbed energy of the aluminum-only beam with equal weight was higher.The composite layup consisting of ±45° layers showed the best performance amongst all considered layups.

The modeling conducted in this work underscores the important influence of hybridization in improving of the mechanical performance of metal components subjected to dynamic loading conditions. The next phase of this research will focus on the validation of the numerical results against experimental data. It is noted that the composite patch considered in this study has the same thickness as the metal alloy constituents. Thicker composite patches will be considered in ongoing work, in particular for the AA7075-T6 hybrids, to examine the variation in peak load and energy absorption as a function of the thickness of the composite reinforcement relative to the metallic component. Moreover, those results will be compared to those for metal-only and composite-only configurations of equal weight.

5 ACKNOWLEDGEMENTS

The authors thank Honda R&D Americas Inc., Arconic Ground Transportation Group, the Natural Sciences and Engineering Research Council (NSERC), the Ontario Centres of Excellence, the Ontario Advanced Manufacturing Consortium, the Ontario Research Fund, the Canada Foundation for Innovation, and the Canada Research Chairs Secretariat for supporting this research.

6 REFERENCES

Abu Talib, A.R., Ali, A., Badie, M.A., Azida Che Lah, N. and Golestaneh, A.F. (2010). Developing a hybrid, carbon/glass fiber-reinforced, epoxy composite automotive drive shaft. Materials & Design, 31(1), 514–521.

Barlat, F., Brem, J.C., Yoon, J.W., Chung, K., Dick, R.E., Lege, D.J., Pourboghrat, F., et al. (2003). Plane stress yield function for aluminum alloy sheets—part 1: theory. International Journal of Plasticity, Elsevier, 19(9), pp. 1297–1319.

Boeriu, H. (2015). Carbon Core body of the new BMW 7 Series wins EuroCarBody Award 2015. available at: https://www.bmwblog.com/2015/11/11/carbon-core-body-of-the-new-bmw-7-series-wins-eurocarbody-award-2015/.

Cao, S., WU, Z. and Wang, X. (2009). Tensile Properties of CFRP and Hybrid FRP Composites at Elevated Temperatures. Journal of Composite Materials, SAGE Publications Ltd STM, 43(4), 315–330.

Chang, F.-K. and Chang, K.-Y. (1987). A Progressive Damage Model for Laminated Composites Containing Stress Concentrations. Journal of Composite Materials, SAGE Publications Ltd STM, 21(9), 834–855.

Dutton, S., Kelly, D. and Baker, A. (2004). Composite Materials for Aircraft Structures, American Institute of Aeronautics and Astronautics.

German, J. and Lutsey, N. (2012). Size or Mass? The Technical Rationale for Selecting Size as an Attribute for Vehicle Efficiency Standards.

Hallquist, J.O. (2013). LS-DYNA® Keyword User's Manual Volume II Material Models, Livermore, California, USA.

HEXCEL. (2016). HexPly 8552 Product Data Sheet, HEXCEL, available at: https://www.hexcel.com/user_area/content_media/raw/HexPly_8552_us_DataSheet.pdf.

Hong, W.-K., Park, S.-C., Kim, J.-M., Kim, S.-I., Lee, S.-G., Yune, D.-Y., Yoon, T.-H. (2010). Development of Structural Composite Hybrid Systems and their Application with regard to the Reduction of CO2 Emissions, Indoor and Built Environment, SAGE Publications Sage UK: London, England, 19(1), 151–162.

Lee, D.G., Sung Kim, H., Woon Kim, J. and Kook Kim, J. (2004). Design and manufacture of an automotive hybrid aluminum/composite drive shaft, Composite Structures, 63(1), 87–99.

Lindberg, H. (2016). Advanced high strength steel technologies in the 2016 Volvo XC90, available at: https://www.autosteel.org/-/media/files/autosteel/great-designs-in-steel/gdis-2016/track-2---volvo-xc90.ashx.

Marsh, G. (2014). Composites and metals–a marriage of convenience?, Reinforced Plastics, Elsevier, 58(2), pp. 38–42.

Neukamm, F., Feucht, M. and Haufe, A. (2009). Considering damage history in crashworthiness simulations, Ls-Dyna Anwenderforum.

Omer, K., ten Kortenaar, L., Butcher, C., Worswick, M., Malcolm, S. and Detwiler, D. (2017). Testing of a hot stamped axial crush member with tailored properties – Experiments and models, International Journal of Impact Engineering, 103, 12–28.

Rahmaan, T., Bardelcik, A., Imbert, J., Butcher, C. and Worswick, M.J. (2016). Effect of strain rate on flow stress and anisotropy of DP600, TRIP780, and AA5182-O sheet metal alloys, International Journal of Impact Engineering, 88, 72–90.

Rahmaan, T., Butcher, C. and Worswick, M.J. (2017). Constitutive Response of AA7075-T6 Aluminum Alloy Sheet in Tensile and Shear Loading BT - Experimental and Applied Mechanics, Volume 4, in Springer International Publishing, Cham, pp. 115–122.

Savage, G. (2010). Formula 1 composites engineering, Engineering Failure Analysis, Elsevier, 17(1), 92–115.

Sun, G., Wang, Z., Hong, J., Song, K. and Li, Q. (2018). Experimental investigation of the quasi-static axial crushing behavior of filament-wound CFRP and aluminum/CFRP hybrid tubes, Composite Structures, 194, 208–225.

Tsai, S.W. and Wu, E.M. (1971). A General Theory of Strength for Anisotropic Materials, Journal of Composite Materials, SAGE Publications Ltd STM, 5(1), 58–80.

Zhu, G., Sun, G., Yu, H., Li, S. and Li, Q. (2018). Energy absorption of metal, composite and metal/composite hybrid structures under oblique crushing loading, International Journal of Mechanical Sciences, 135, 458–483.